


## Article

# Pyrolysis of Cyclohexane and 1-Hexene at High Temperatures and Pressures—A Photoionization Mass Spectrometry Study

Robert S. Tranter <sup>1,\*</sup>, Colin Banyon <sup>1</sup>, Ryan E. Hawtof <sup>2</sup> and Keunsoo Kim <sup>1</sup>

<sup>1</sup> Chemical Sciences and Engineering Division, Argonne National Laboratory, 9700 S. Cass Ave., Lemont, IL 60439, USA

<sup>2</sup> Department of Chemical Engineering, Massachusetts Institute of Technology, 77 Massachusetts Ave., Cambridge, MA 02139, USA

\* Correspondence: tranter@anl.gov

**Abstract:** Cycloalkanes are important components of a wide range of fuels. However, there are few experimental data at simultaneously high temperatures and pressures similar to those found in practical systems. Such data are necessary for developing and testing chemical kinetic models. In this study, data relevant to cycloalkane pyrolysis were obtained from high repetition rate shock tube experiments coupled with synchrotron-based photoionization mass spectrometry diagnostics. The pyrolysis of cyclohexane was studied over 1270–1550 K and ~9 bar, while the more reactive primary decomposition product, 1-hexene, was studied at 1160–1470 K and ~5 bar. Insights into the decomposition of the parent molecules, the formation of primary products and the production of aromatic species were gained. Simulations were performed with models for cyclohexane and 1-hexene that were based on literature models. The results indicate that over several hundred microseconds reaction time at high pressures and temperatures the pyrolysis of cyclohexane is largely dominated by reactions initiated by cyclohexyl radicals. Furthermore, good agreement between the simulations and the experiments were observed for cyclohexane and 1-hexene with a modified version of the cyclohexane model. Conversely, the 1-hexene model did not reproduce the experimental observations.

**Keywords:** shock tubes; chemical kinetic simulations; cycloalkanes; 1-alkenes; time-of-flight mass spectrometry



**Citation:** Tranter, R.S.; Banyon, C.; Hawtof, R.E.; Kim, K. Pyrolysis of Cyclohexane and 1-Hexene at High Temperatures and Pressures—A Photoionization Mass Spectrometry Study. *Energies* **2023**, *16*, 7929. <https://doi.org/10.3390/en16247929>

Academic Editors: Marina Braun-Unkhoff and Sandra Richter

Received: 9 October 2023

Revised: 17 November 2023

Accepted: 25 November 2023

Published: 6 December 2023

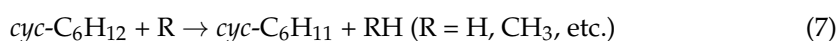


**Copyright:** © 2023 by the authors. Licensee MDPI, Basel, Switzerland. This article is an open access article distributed under the terms and conditions of the Creative Commons Attribution (CC BY) license (<https://creativecommons.org/licenses/by/4.0/>).

## 1. Introduction

Practical fuels, including some sustainable aviation fuels, contain a wide range of cycloalkanes and substituted cycloalkanes. Consequently, decomposition of cycloalkanes is a critical step in the formation of the radical pool in combustion and pyrolysis systems. Optimizing usage of fuels requires accurate chemical kinetic models that span a broad range of operating conditions, but data are often lacking under practical conditions. With respect to gas phase chemistry, cyclohexane is one of the most studied cycloalkanes, which, as well as being a fuel component, is often used as a surrogate for monocycloalkanes [1–3]. Consequently, accurate mechanisms, preferably validated against experimental targets, describing the gas phase chemistry of cyclohexane are necessary for models to reliably predict the behavior of systems over a broad range of conditions. Obtaining experimental data at the high temperatures and pressures characteristic of combustors is challenging, and detailed studies of the pyrolysis of cyclohexane at simultaneously high temperatures and pressures are sparse.

Dissociation of cyclohexane, *cyc*-C<sub>6</sub>H<sub>12</sub>, is initiated by ring opening, reaction (1), to form a diradical that rapidly isomerizes to 1-hexene (1-C<sub>6</sub>H<sub>12</sub>), reaction (2). The subsequent reactions of 1-hexene and its products drive the secondary chemistry, rapidly producing H-atoms and CH<sub>3</sub> radicals, which attack cyclohexane. H-abstraction, reaction (7), from cyclohexane can be competitive with ring opening [4].



Various methods have been used to study pyrolysis of cyclohexane. Tsang [4] used the single pulse shock tube method (1000–1200 K, 2–7 bar, residence time ~800  $\mu\text{s}$ ) and measured the concentrations of stable pyrolysis products from cyclohexane and 1-hexene. Tsang determined that 1-hexene was a major product from cyclohexane and that several of the observed products had to be formed from the cyclohexyl radical. Brown et al. [5] confirmed many of Tsang's observations concerning the mechanism using very low pressure pyrolysis, 900–1200 K. In a comprehensive experimental shock tube/laser schlieren densitometry (1300–2000 K, 33–267 mbar, reaction time < 10  $\mu\text{s}$ ), and theoretical study of the very early stages of cyclohexane pyrolysis, Kiefer et al. [6] confirmed that ring opening of cyclohexane, ultimately yielding 1-hexene, was the sole initiation reaction. The laser schlieren experiments were extremely sensitive to reactions (1) and (2) but largely insensitive to reaction (7). While Kiefer et al. and Brown et al. agreed with Tsang about the mechanism for pyrolysis of cyclohexane, they disagreed with Tsang on the rate coefficient of reaction (1),  $k_1$ . Peukert et al. [7] used the H-ARAS technique (1320–1550 K, 1.8–2.2 bar, reaction time ~1 ms) behind reflected shock waves and reached similar conclusions to Tsang regarding the pyrolysis mechanism and the value of  $k_1$ . More recently, two flow reactor studies between 900 K and 1500 K by Wang et al. [8] at 40 mbar and Khandavilli et al. [9] at 1700 mbar further confirmed Tsang's observations regarding the mechanism. Wang et al. [8] used a flow reactor coupled via molecular beam sampling to a photoionization mass spectrometer (PIMS) with tunable synchrotron vacuum ultraviolet (SVUV) as the ionizing radiation. The results included concentration/temperature plots at a fixed reaction time and allowed isomers to be distinguished for some species. Khandavilli et al. [9] obtained similar datasets to Wang but identified stable species using gas chromatography.

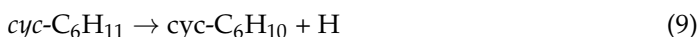
The only high pressure and temperature study of cyclohexane pyrolysis is one by Lyszka and Brezinsky [10] who used a single pulse shock tube (950–1650 K, ~2.2 ms) to obtain stable species concentrations at reaction pressures up to 200 bar. An important aspect of this work was to examine the effect of pressure and initial fuel concentration on the product distributions. This demonstrated that fuel concentration was a key factor in determining the reaction product distributions. Furthermore, the study highlighted deficiencies in the ability of literature models to predict several important species, including benzene, accurately at elevated pressures.

Using the same experimental methods as for their cyclohexane studies Tsang (980–1170 K, 1.7–5.3 bar) [4], Kiefer et al. (1220–1700 K, 60 and 263 mbar) [6] and Peukert et al. (1250–1380 K, 1.5–2.5 bar) [7] also studied the dissociation of 1-hexene. They all concluded that the primary initial dissociation reaction was breaking of the allylic C–C bond, reaction (3). Recently, Fan et al. [11] studied the pyrolysis of 1-hexene in a flow reactor over 800–1350 K. Two diagnostics were used: (1) SVUV PIMS at 40 mbar reaction pressure; (2) gas chromatography/mass spectrometry for pressures of 0.04–1 bar.

Most of the experimental work has been complemented by theoretical studies [6,12–14]. These reaffirm the dominance of reactions (1) and (2) at high temperatures, but other minor ring opening pathways were also proposed that may be accessible at high temperatures.

Kiefer et al. also provided RRKM calculations for several key steps and Zsély et al. [15] produced an optimized model for cyclohexane based on experiments in the literature.

The importance of reaction (7), H-abstraction as a source of cyclohexyl radicals, was initially addressed by Tsang [4] and later supported by Wang et al. [8]. Three paths were proposed for the loss of the cyclohexyl radical: ring opening to an unsaturated radical (reaction (8)); dehydrogenation to cyclohexene (reaction (9)); isomerization to a cyclopentylmethyl radical (reaction (10)).



Recent theoretical works by Knepp et al. [16] and Gong et al. [13] support the ring opening and dehydrogenation channels for pyrolysis of cyclohexyl. However, they also suggest that isomerization of 1-C<sub>6</sub>H<sub>11</sub>-6 generates the cyclopentylmethyl radical rather than it being formed directly by reaction (10).

Wang et al. [8] developed a detailed chemical kinetic model for cyclohexane pyrolysis that satisfactorily reproduced their experimental results. The model was later updated and embedded as a sub-mechanism in a detailed model for methylcyclohexane (MCH) combustion [17]. Liszka and Brezinsky [10] later extended the MCH mechanism to 200 bar and through a Monte Carlo-based optimization approach identified and modified three reactions that improved predictions of benzene formation at very high pressures.

Prior literature on cyclohexane and 1-hexene pyrolysis provides a solid understanding of the initiation steps and secondary chemistry despite some disagreement on key rate coefficients. However, none of the experimental studies provide time-resolved speciation data at high pressure (P) and high temperature (T) simultaneously. In the current work, time-resolved SVUV/PIMS data, similar to the low-pressure data of Wang et al. [8] and Fan et al. [11], were obtained for pyrolysis of cyclohexane and 1-hexene. However, rather than P = 40 mbar the reaction pressures of this work were ~5 bar (1-hexene) and ~9 bar (cyclohexane). For cyclohexane, the reaction temperatures encompass the range of Wang et al. [8] and the lower end from Kiefer et al. [6]. The 1-hexene studies were performed at lower temperatures and overlap the lower range of the cyclohexane work. The time-resolved speciation data provide insights into the dissociation of cyclohexane and 1-hexene at conditions relevant to practical combustion devices.

## 2. Methods

### 2.1. Experiments

The pyrolysis of cyclohexane and 1-hexene were studied behind reflected shock waves. Conditions were selected such that no reaction occurred during the incident shock wave and that the heating time in the reflected shock ( $\ll 1 \mu\text{s}$ ) was considerably shorter than the reaction period ( $>300 \mu\text{s}$ ). Cyclohexene was studied over the range  $T_5 = 1270\text{--}1550 \text{ K}$  and  $P_5 = 6.9\text{--}11.5 \text{ bar}$  where  $T_5$  and  $P_5$  are the temperature and pressure behind the reflected shock wave, i.e., the initial reaction conditions. The experiments with 1-hexene spanned  $T_5 = 1160\text{--}1470 \text{ K}$  and  $P_5 = 4.4\text{--}6.3 \text{ bar}$ . The experiments were performed in the Argonne high-repetition rate shock tube (ANL-HRRST) which was coupled via a differentially pumped molecular beam sampling (MBS) interface to a time-of-flight mass spectrometer (TOF-MS) [18]. The ANL-HRRST/TOF-MS has been extensively described previously [18–20]. Briefly, it is a miniature shock tube and was primarily designed for experiments at user facilities such as synchrotron beamlines. The driven section has a bore of just 6.35 mm and a total length of 880 mm. The driver section is a high-pressure solenoid valve. The ANL-HRRST is fully automated, and experiments were conducted at a repetition rate of 1 Hz, i.e., one shock per second. The methodology for data collection and analysis was similar to recent studies on alkyl radical recombination [21,22] and styrene

dissociation [18]. The temperatures and pressures behind the incident and reflected shock waves were obtained from the incident shock velocity, the mixture composition and  $P_1$ , the pressure to which the driven section was filled with reagent mixture, and the standard shock wave equations assuming ideal gas behavior [23,24]. The shock velocities were obtained from six piezoelectric pressure transducers (Dynasen, CA-1136) installed in the side of the driven section, 50.0 mm between centers. There was 75 mm between the last pressure transducer and the nozzle that formed the entrance to the MBS interface. The shock velocity at the nozzle was obtained using extrapolation. The uncertainties in the incident shock velocities are estimated as 0.2%, which corresponds to an uncertainty in temperature of  $\sim 0.5\%$  or less than  $\pm 10$  K per experiment. For each experimental condition ( $T_5$  and  $P_5$ ) mass spectra from many experiments were averaged. The average  $T_5$  and  $P_5$  with uncertainties are given in Tables 1 and 2. Throughout the remainder of the manuscript the nominal  $T_5$  from Tables 1 and 2 are used to refer to an experimental set.

**Table 1.** Reaction conditions for 0.125% cyclohexane/argon.

$T_5$ /K (Nominal)	$T_5$ /K (Mean)	$\sigma$ $T_5$ /K <sup>a</sup>	$P_5$ /bar	$\sigma$ $P_5$ /bar <sup>a</sup>	MgF <sub>2</sub> Filter
1270	1264	16.37	6.87	0.15	N
	1277	15.60	6.96	0.15	Y
1340	1333	14.30	7.46	0.14	N
	1340	13.04	7.54	0.13	Y
1400	1394	16.06	8.01	0.15	N
	1408	16.73	8.12	0.16	Y
1480	1487	17.60	8.84	0.18	N
	1472	18.64	8.71	0.18	Y
1550	1541	20.43	9.39	0.20	N
	1563	20.96	9.56	0.20	Y

<sup>a</sup>  $\sigma$  = standard deviation.

**Table 2.** Reaction conditions for 0.25% 1-hexene/argon.

$T_5$ /K (Nominal)	$T_5$ /K (Mean)	$\sigma$ $T_5$ /K <sup>a</sup>	$P_5$ /bar	$\sigma$ $P_5$ /bar <sup>a</sup>
1160	1157	19.7	4.41	0.14
1360	1364	16.76	5.80	0.13
1470	1445	17.97	6.39	0.14

<sup>a</sup>  $\sigma$  = standard deviation.

The experiments were performed at the Chemical Dynamics Beamline (9.0.2) of the Advanced Light Source. The molecular beam from the ANL-HRRST was intersected by highly tunable vacuum ultraviolet (VUV) photons in the ionization zone of the mass spectrometer to create cations that were extracted into the flight tube of the TOF-MS. Beamline 9.0.2 is equipped with four endstations with different VUV beam properties. The cyclohexane experiments were performed at the T2 endstation, whereas the 1-hexene work was conducted at T4 in a later experimental campaign. The T4 endstation is equipped with a monochromator that produces high resolution VUV (35 meV bandwidth, 600  $\mu$ s slit width [25]). T2 is not equipped with a monochromator and photon energies (PE) were obtained by directly adjusting the undulator gap. The bandwidth at T2 was broader (0.3 eV) than at T4 although still adequate for this work. The flux at T2 is approximately 1000 times greater than at T4 and less signal averaging is necessary at T2 to obtain adequate signal/noise (S/N). The light emitted by the undulator contains not only photons at the desired PE but also photons at higher harmonic energies. The high-energy photons were largely, but not entirely, removed by an argon gas filter that served both T2 and T4. The T4 monochromator effectively removed the residual high-energy photons producing very

clean light at T4. The challenges encountered at T2 due to the residual high harmonic photons have been previously discussed, along with mitigation strategies that involved the use of a MgF<sub>2</sub> filter [21,22] with a cutoff at 11.2 eV. A similar approach was used in the cyclohexane work where pairs of experiments with the filter (PE = 7.75–10.75 eV, 0.5 eV steps) and without the filter (PE = 7.75–12.00 eV, 0.25 eV steps) were conducted. At each PE, 100 experiments were ensemble averaged. With 1-hexene at T4, 500 experiments were signal averaged to compensate for the reduced photon flux (PE = 9.70–11.00 eV, 0.1 eV steps). An additional dataset was collected from T4 at 13.5 eV to allow species with IE >11.00 eV to be detected.

For all experiments mass spectra were collected at 10 μs intervals for a 3 ms period that spanned from before and after formation of the reflected shock wave. The resulting datasets consist of three independent variables (mass (*m/z*), reaction time (*t*) and PE) and one dependent variable, the signal intensity (*S*). The data were post-processed according to the methodologies detailed in Refs. [18,22], and baseline corrections were made using the algorithm described in [22]. The relationship between *S* and the concentration of a species, *X*, is given by the following expression.

$$S = C X M_d \sigma_{xeV}$$

*C* is the product of several instrument constants that are independent of mass, *M<sub>d</sub>* is the mass discrimination factor and  $\sigma_{xeV}$  is the photoionization cross-section for a species at a specific PE. As previously, *M<sub>d</sub>* is assumed to be unity [21]. Similar to prior studies [21,22], it is not possible to convert *S* into absolute concentrations due to a lack of a suitable internal standard to account for pressure changes in the ion source of the mass spectrometer. Consequently, concentrations will be referred to as effective concentrations, *X<sub>eff</sub>*. However, accurate relative concentrations and branching [21] fractions can be obtained by taking ratios of *X<sub>eff</sub>*. *C* is dependent on the flux of the VUV photon beam, which in turn is a function of the storage ring current in the synchrotron and the selected photon energy. During the cyclohexane and 1-hexene experiments the storage ring current fluctuated slowly and could be as low as 65% of the normal stable operating value. Consequently, the effective concentrations of species are normalized by the ratio of an average value from the pre-shock signal for *m/z* 84 (the parent ion of cyclohexane and 1-hexene) to the averaged pre-shock *m/z* 84 value from a reference experiment. For cyclohexane, the 1270 K dataset was used as the reference and for 1-hexene, the 1160 K dataset was selected.

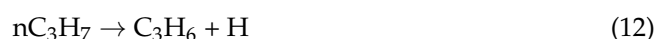
Three projections of the data are particularly useful in the current study and are used throughout the remainder of this paper. First, selected mass peaks were integrated over the first 1500 μs after shock arrival at each PE. This created mass-selected photoionization spectra (PIE) and allowed species to be identified by both *m/z* and the ionization threshold (IE). Additionally, the shape of the PIE spectrum can be used to distinguish isomers. It should be noted that the PIE spectra obtained here are relatively low-resolution due to the step sizes and bandwidth of the light source. Nonetheless, they are suitable for distinguishing some isomers and species of the same mass but different composition, see for example [21]. Second, *S* vs. *t*, equivalent to concentration/time, were extracted for selected masses. These were subsequently scaled by  $\sigma_{xeV}$  ([26–38] and Table S1) to obtain *X<sub>eff</sub>*. These plots reveal both the order of appearance of products as well as their relative abundance. Third, *S* vs. *m/z* plots are equivalent to classical mass spectra.

Reagent mixtures were created on the fly using a novel mixing apparatus which has been fully described previously [39]. Reagent mixtures containing 0.125% cyclohexane (Sigma-Aldrich, St. Louis, MO, USA 99.5%) or 0.25% 1-hexene (Sigma-Aldrich, St. Louis, MO, USA 99%) diluted in argon (Airgas, Berkeley, CA, USA grade 5.0) were prepared.

## 2.2. Simulations

Chemical kinetic simulations were performed with an in-house program, Frhodo [40]. The reflected shock reaction zone was modeled as a 0D constant pressure reactor. The chemical kinetic model used was Wang's methylcyclohexane (MCH) model [17] with the

updates from Liska and Brezinsky [10]. The MCH model was designed for combustion simulations and contains many reactions that are superfluous to pyrolysis. Consequently, the MCH model was reduced by stripping out all reactions involving oxygenated species and atomic or molecular oxygen. Simulations of cyclohexane pyrolysis with the original and reduced MCH model were essentially identical. The reduced MCH model was further modified to replace rate parameters for the multi-channel unimolecular dissociation of 1-hexene with the recent theoretical results from Wang [41]. Wang did not calculate rate coefficients for reaction (6), the retroene dissociation to two propene molecules. Consequently, the parameters for reaction (6) were retained from the MCH model. The dissociation and isomerization reactions of 1,3-butadiene and the other  $C_4H_6$  isomers was updated based on the master equation model from Lockhart et al. [42]. The rate coefficient expressions for dissociation of the *n*-propyl radical, reactions (11) and (12), were updated with PLOG expressions from Miller et al. [43].



The reduced MCH model with the above changes will be referred to as MCHb. A more recent model for only 1-hexene was published by Fan et al. [11]. Consequently, the 1-hexene experiments were simulated with both the MCHb and the Fan model. Reaction flux analyses were performed using Cantera 2.6 [44] and the results visualized with PyDot 1.4.2 [45] and GraphViz 9.0.0 [46].

### 3. Results

#### 3.1. Cyclohexane

Shown in Figure 1 are example mass spectra from the dataset at 1400 K and 8 bar without the  $MgF_2$  filter. Use of the filter significantly attenuated the flux resulting in weaker signals and reduced S/N. Comparison of the datasets with and without the filter showed that dissociative ionization due to the residual high harmonic light was mostly of minor importance in the cyclohexane studies. Consequently, data are shown from the experiments without the filter, unless noted otherwise. The data in Figure 1 were obtained with PE = 10.75 eV and the spectra cover the pre-shock region and two intervals after the reflected shock. At 10.75 eV cyclohexane should not dissociatively ionize [32] and only a single peak should be observed in the pre-shock mass spectrum in Figure 1. The minor peak at  $m/z$  56 can be attributed to dissociative ionization (DI) induced by high-energy photons that were not removed by the gas filter. At 300  $\mu s$  reaction time the principal products are ethene (28) and 1,3-butadiene (54) and the minor products included  $C_3H_4$  (40) and  $C_3H_6$  (42). At longer times additional peaks appear, including  $C_5H_6$  (66), benzene (78) and even traces of larger aromatics such as phenyl acetylene (102), styrene  $C_8H_8$  (104), and  $m/z$  116 and 128 which could be indene and naphthalene, respectively. Ethyne was not detected, and the maximum PE was below the IE of methane. Over the range of experimental conditions, the products observed remain essentially the same and it is mainly the extent of reaction that changes with temperature for a fixed observation time. This is illustrated in Figure 2, where 10.75 eV mass spectra at 300  $\mu s$  post-shock from experiments at three different temperatures are shown. The 1550 K data in Figure 2 are similar to the 1500  $\mu s$  data in Figure 1. In Figure 3 the effective concentration of 1,3-butadiene is plotted for a range of temperatures. At lower temperatures, the formation of 1,3-butadiene is slow, consistent with slow dissociation of cyclohexane. At higher temperatures, 1,3-butadiene is produced rapidly, but above 1400 K the concentration reaches a maximum and drops at longer times as 1,3-butadiene is consumed. Similar plots for propene, allene + propyne and ethene are given in Figures S1–S3 of the supplemental material.

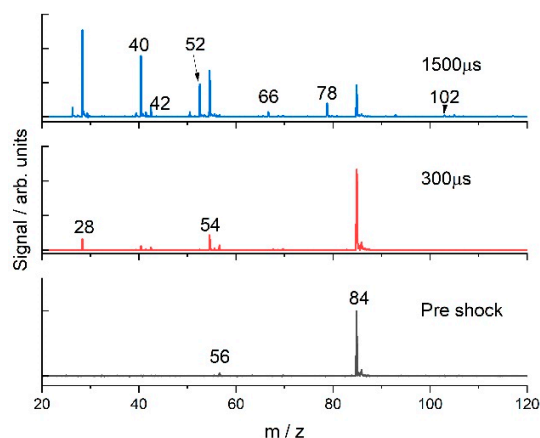


**Figure 1.** Mass spectra from pyrolysis of cyclohexane; 1400 K, 8 bar, 10.75 eV, no  $\text{MgF}_2$  filter.

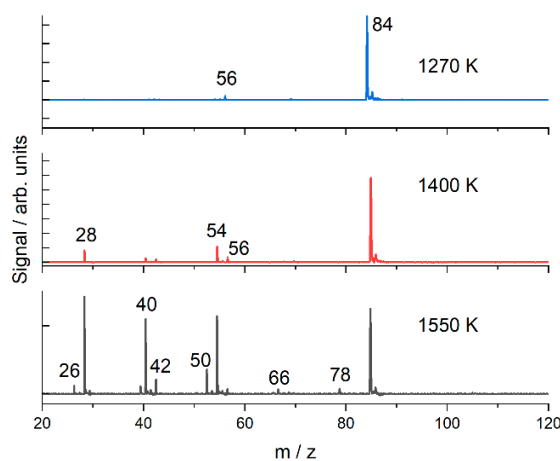


**Figure 2.** Mass spectra from pyrolysis of cyclohexane; 300  $\mu\text{s}$  reaction time, 10.75 eV, no  $\text{MgF}_2$  filter.

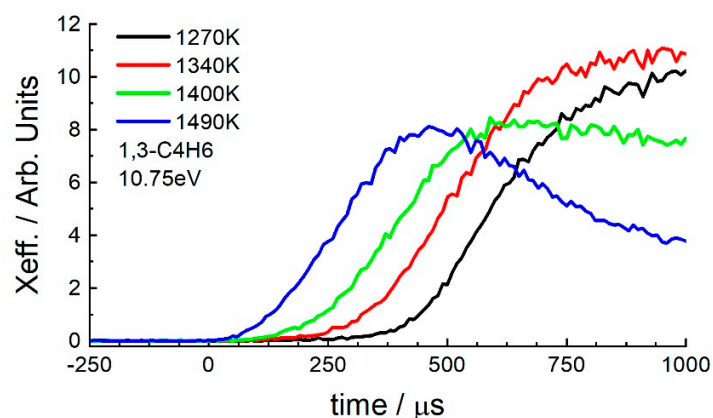


**Figure 3.** Effective concentrations of 1,3-butadiene from the pyrolysis of cyclohexane at various temperatures,  $\sim 8$  bar, 10.75 eV, no  $\text{MgF}_2$ .  $t = 0$  corresponds to formation of the reflected shock wave.

In Figure 4, plots of  $X_{\text{eff}}$  against time at 10.75 eV, 1400 K and 8 bar, for several key stable species are shown. Negative values on the X-axis represent the period before the formation of the reflected shock wave (time = 0) which initiates reaction. Ethene is the dominant species. At 300  $\mu\text{s}$  ethene is about 1.8 times more abundant than 1,3-butadiene. The species in order of decreasing concentration are ethene > 1,3-butadiene > propene >  $m/z$  40. PE = 10.75 eV is above the ionization thresholds of allene and propyne [32] and the observed  $X_{\text{eff}}$  at  $m/z$  40 is the sum of their concentrations. Ethene and 1,3-butadiene are

initially formed at the same time, almost immediately following shock reflection. Propene appears a little later, followed by  $m/z$  40. The trends in the order of appearance of species and their relative concentrations are similar to the other reaction conditions studied. The major differences being that at lower temperatures the appearances of species are delayed relative to time = 0, and at higher temperatures 1,3-butadiene is consumed more rapidly. In all cases ethene is the major species.

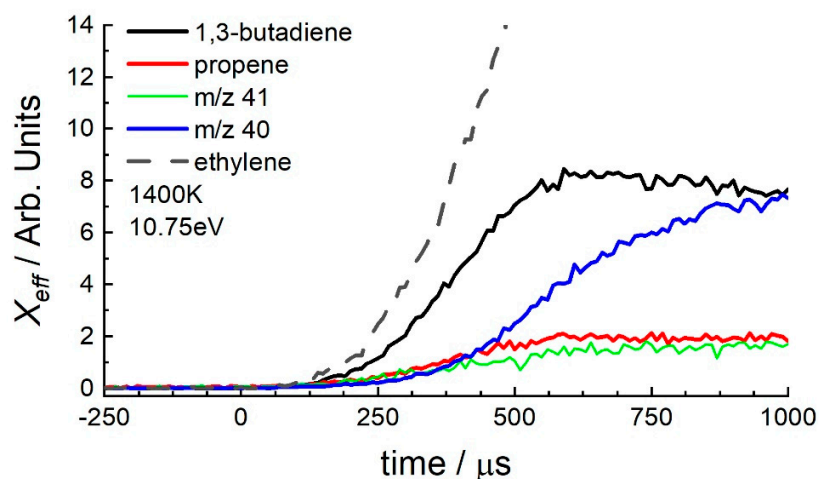


**Figure 4.** Effective concentrations of key species from the dissociation of cyclohexane at 8 bar. No  $MgF_2$  filter.  $m/z$  40 = allene + propyne.  $m/z$  41 = allyl +  $^{13}C$  from  $m/z$  40.  $t = 0$  corresponds to formation of the reflected shock wave.

In Figure 5, PIE spectra for the masses corresponding to the species in Figure 4 are shown. There is good agreement between the appearance energies for most of the species and literature values of ionization energies (IE): 1,3-butadiene ( $m/z$  54, IE 9.072 eV [32]), propene ( $m/z$  42, IE 9.73 eV [32]) and ethene ( $m/z$  28, IE 10.5138 eV [32]). There is some ambiguity in assigning a single  $C_3H_4$  species to  $m/z$  40. At lower energies the  $m/z$  40 curve is solely due to allene ( $m/z$  40, IE 9.692 eV [32]). However, at higher energies the curve is likely composed of allene and propyne ( $m/z$  40, IE 10.36 eV [32]) as isomerization between the two is reasonably facile at the temperatures of the current work [47]. Thus,  $m/z$  40 will be considered as a mixture of allene and propyne for  $PE > 10.4$  eV. There is also some difficulty assigning  $m/z$  41 which might be expected to be allyl ( $C_3H_5$ ). The temporal behavior in Figure 4 shows  $m/z$  41 and propene being formed simultaneously and  $m/z$  41 persisting to long time. However, the time profile of a radical species, even a resonantly stabilized one such as allyl, would be expected to exhibit a peak at relatively low concentrations, as the radical is formed and rapidly consumed. Close inspection of Figure 5 shows a small increase in the  $m/z$  41 signal at around 8.2 eV, which is consistent with the IE = 8.13 eV for the allyl radical [48]. However, at about 10.75 eV there is a sharp increase in the signal after which  $m/z$  41 tracks  $m/z$  42. This suggests that at 10.75 eV propene is dissociatively ionizing to  $m/z$  41 which should not occur until about 11.8 eV [32]. Similar to the appearance of  $m/z$  56 in the pre-shock mass spectrum, Figure 1, the behavior of  $m/z$  41 in Figures 4 and 5 strongly suggest the trace in Figure 4 is mainly from photodissociation of propene by residual high harmonic light rather than ionization of allyl radicals. However, an accurate  $m/z$  41  $X_{eff}/time$  profile was obtained, Figure 6, at  $PE = 10.00$  eV with the  $MgF_2$  filter. The filter effectively blocks photons in excess of 11.2 eV, preventing dissociative ionization of propene. The  $m/z$  41 signal shows the expected rise and fall, and the maximum propene signal (not shown) is at least a factor of 4 greater than that of  $m/z$  41. The  $^{13}C$  isotopologue of allene also contributes to the  $m/z$  41 signal. However, as shown in Figure 6, the fraction of  $m/z$  41 due to  $^{13}C$  (3.3% of allene) is nearly negligible. Thus, the  $m/z$  41 signal in Figure 6 represents  $X_{eff}$  of the allyl radical at 10.00 eV.



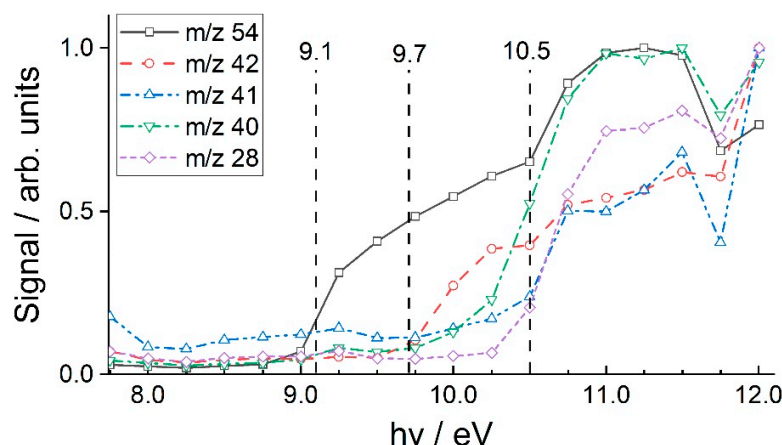


**Figure 5.** Mass-selected photoionization spectra corresponding to Figure 4. Vertical lines indicate approximate locations of ionization thresholds (see text for exact values).

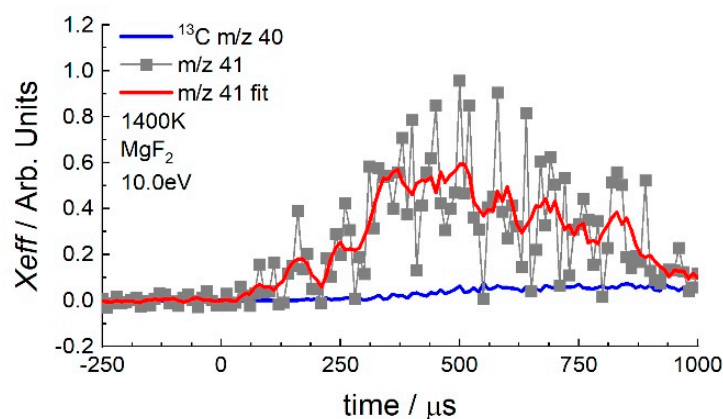


**Figure 6.** Effective concentration of the allyl radical produced from dissociation of cyclohexane. PE = 10.0 eV, with the MgF<sub>2</sub> filter. m/z 41 is corrected for the <sup>13</sup>C isotopologue of m/z 40. The red line is a best fit to the m/z 41 signal as a visual aid. t = 0 corresponds to formation of the reflected shock wave.

From prior studies, the initial dissociation of cyclohexane proceeds via reactions (1) and (2), yielding 1-hexene. Tsang identified 1-hexene as the major product [4] and Wang et al. [8] identified it in the photoionization spectrum for m/z 84 where it was distinguishable from the isomer cyclohexane. In Figure 7, PIEs for m/z 84 are shown from experiments at 1270 K and 1400 K, slightly lower than the 1440 K of the m/z 84 PIE in Ref. [8]. The IE of 1-hexene is 9.44 eV [32] and that of cyclohexane is 9.88 eV [32]. In Figure 7 there is no indication of an increase in signal in the region of 9.4 eV and at both temperatures the PIE spectra are essentially identical.

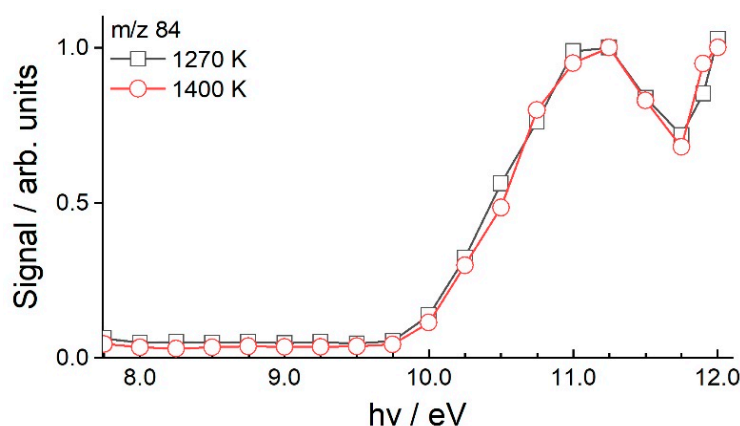


**Figure 7.** Photoionization spectra for  $m/z$  84 from the dissociation of cyclohexane at two temperatures.

### 3.2. 1-Hexene

The pyrolysis of 1-hexene was studied at 1160–1470 K and pressures of 4.4–6.4 bar at the T4 endstation. Example mass spectra at 10.70 eV are shown in Figures 8 and 9. There is a small peak at  $m/z$  56 and a very minor peak at  $m/z$  69 (clearer in the 300  $\mu$ s image, Figure 8) in the pre-shock mass spectrum. These peaks indicate a small amount of dissociative ionization of 1-hexene and are consistent with Yang et al. [27]. The data in Figure 8 indicate that at 1160 K and 4.4 bar dissociation of 1-hexene is slow. After 300  $\mu$ s there is little reaction, although small product peaks can be discerned, e.g.,  $m/z$  28. Like cyclohexane, there appears to be little change in the products from 1-hexene as the reaction temperature changes. In Figure 9 mass spectra are shown after 300  $\mu$ s reaction at 1160, 1360 and 1470 K and the 1360 K spectrum is similar to the 1160 K, 1000  $\mu$ s plot in Figure 8.

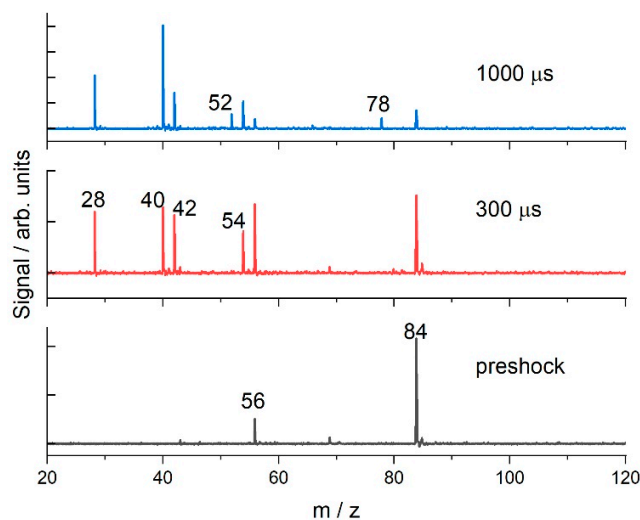


**Figure 8.** Mass spectra from the dissociation of 1-hexene; 1160 K, 4.4 bar, 10.70 eV.

In Figure 10  $X_{eff}$ /time plots (PE = 10.70 eV) of 1-hexene and the main products at 1160 K are shown. Figure S4 of the supplementary material shows similar data from experiments at 1360 K. The 1-hexene signal rises steadily due to the pressure increase in the ionization region after reflection of the shock wave ( $t = 0$ ) before decaying. The products first appear at about 200  $\mu$ s consistent with slow dissociation of 1-hexene. Ethene is the dominant product similar to the pyrolysis of cyclohexane. 1-Butene and propene are the second largest products and have similar  $X_{eff}$ . The 1-butene profile in Figure 10 has been corrected to remove contributions from DI of 1-hexene, which is approximately 18% of the  $m/z$  84 signal at 10.70 eV [27]. Allene/propyne and 1,3-butadiene are also of similar  $X_{eff}$  and a factor of 3.5 smaller than propene and 1-butene. Additional species detected

include benzene, cyclopentadiene, vinylacetylene, propargyl radical, ethyne and methane. No aromatics larger than benzene were observed.

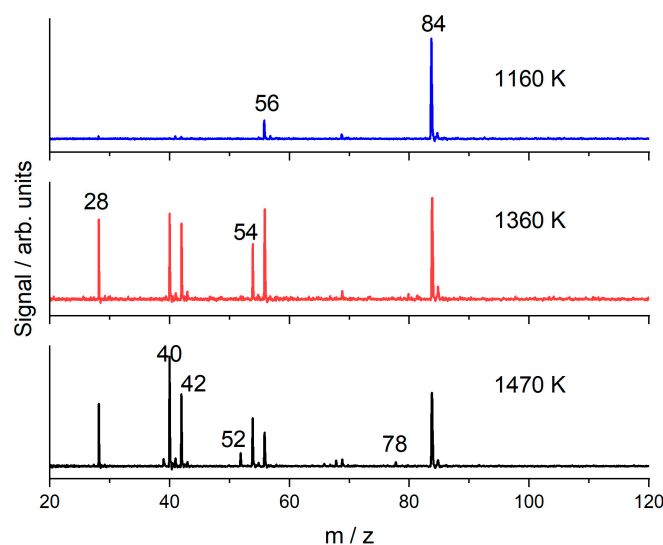


**Figure 9.** Mass spectra from the dissociation of 1-hexene at various temperatures and 4.4–6.4 bar; 300  $\mu$ s reaction time, 10.70 eV.

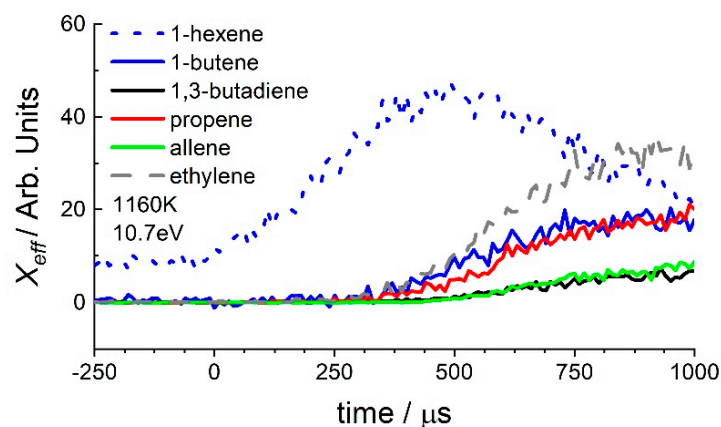


**Figure 10.** Effective concentrations of 1-hexene and the main products; 1160 K and 4.4 bar.  $t = 0$  corresponds to formation of the reflected shock wave.

The 10.00 eV allyl radical  $X_{eff}$ /time profile is shown in Figure 11 for 1160 K and 4.4 bar. The data are corrected for the minor contribution due to the  $^{13}\text{C}$  isotopologue of allene. In contrast to the cyclohexene experiments, which were conducted at T2, DI of propene does not contribute to the  $m/z$  41 signal. The plot shows a slow steady increase in  $X_{eff}$ , indicating that reactions consuming allyl are slow relative to its rate of formation. At 1360 K, see Figure S5 in the supplementary material, the allyl radical signal shape is similar to that in Figure 6, cyclohexane (1400 K).

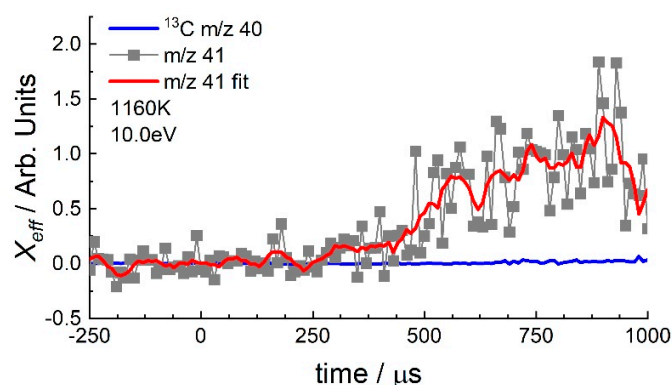


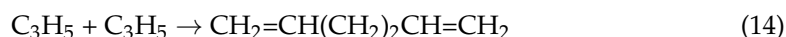
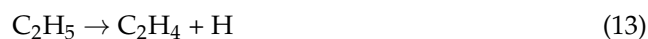
**Figure 11.** Effective concentration of the allyl radical produced from dissociation of 1-hexene; 1160 K and 4.4 bar, PE = 10.0 eV.  $m/z$  41 is corrected for the  $^{13}\text{C}$  isotopologue of  $m/z$  40. The red line is a best fit to the  $m/z$  41 signal as a visual aid.  $t = 0$  corresponds to formation of the reflected shock wave.

#### 4. Discussion

The initial dissociation reactions of cyclohexane and 1-hexene are mainly simple C-C bond scissions. Cyclohexane forms a diradical, reaction (1), which rapidly isomerizes to 1-hexene, and 1-hexene splits at the allylic C-C bond to give  $n$ -propyl and allyl radicals, reaction (3). Kiefer et al. [6] commented that at short times in laser schlieren/shock tube experiments ( $<10 \mu\text{s}$ ) the chemistry of cyclohexane is largely that of 1-hexene. However, at longer reaction times, e.g., Tsang [4] ( $\sim 800 \mu\text{s}$ ), the products formed are from a more complicated set of secondary reactions arising from attack on the parent molecule by radical species formed from the initial dissociation products. Chemical kinetic modeling has been used to explore routes of formation of the products and compare the predictions of ratios of mole fractions with ratios of experimental  $X_{\text{eff}}$ . Due to the importance of 1-hexene as a primary product of cyclohexane it will be discussed first.

##### 4.1. 1-Hexene

Based on the literature, dissociation of 1-hexene in the current work mostly proceeds by reaction (3) to give allyl and  $n$ -propyl radicals. The  $X_{\text{eff}}$  for allyl is shown in Figure 10 at the lowest temperature studied. In these experiments the  $n$ -propyl radical could not be observed, although it was previously seen in HRRST/TOF-MS experiments by Banyon et al. at much lower reaction temperatures [22]. From a theoretical study of reactions on the  $\text{C}_3\text{H}_7$  potential energy surface Miller and Klippenstein [43] calculated that  $k_{11} > 10^7 \text{ s}^{-1}$  and  $k_{12} > 10^5 \text{ s}^{-1}$  over the experimental range. In the MCHb model,  $k_{11}$  and  $k_{12}$  are from the 1991 evaluation by Tsang [49] and those in the Fan mechanism are from Hansen et al. [50]. At 1160 K and 4.4 bar Tsang's  $k_{11}$  is a factor of 3 lower than Miller and Klippenstein's value and  $k_{12}$  is a factor of 2 lower, which will reduce the rate of production of  $\text{CH}_3$  and  $\text{H}$ . From Hansen,  $k_{11}$  is similar to Tsang but  $k_{12}$  is about a factor of 40 lower than from Miller and Klippenstein. Thus,  $n$ -propyl radicals will dissociate too rapidly to be observed in these experiments and predominantly generate ethene and methyl radicals. A small fraction of these radicals will yield propene and H-atoms, although this will be negligible in the Fan model.



Reaction (3), yielding allyl and  $n$ -propyl radicals, is the dominant route for dissociation of 1-hexene. However, reaction flux analysis (Figures S6 and S7 of the supplementary

material) indicates that in the Fan model reaction (4) yielding  $C_2H_5 + nC_4H_7$  radicals has a small but noticeable flux. In both the Fan and MCHb models, reaction (5), forming  $CH_3 + PXC_5H_9$  radicals, is also a minor but significant route consuming 1-hexene. The three non-methyl radicals rapidly dissociate ( $k > 10^7 s^{-1}$ ) yielding H-atoms. Thus, although the channels are minor compared to reaction (3), they are an early source of H-atoms that become more competitive at higher temperatures, e.g.,  $k_3/k_4 = 38$  at 1160 K and 22 at 1360 K. These H-atoms are necessary for promoting H-abstraction reactions from 1-hexene, which have similar fluxes in both models. Reaction (6), the retroene dissociation of 1-hexene, is also a significant route consuming 1-hexene and is approximately twice as important in the MCHb model compared to the Fan model.

At 1160 K, the allyl radical is stable ( $k_{17} \sim 370 s^{-1}$ ) [51]) and is removed mainly through addition reactions. Recombination of allyl radicals to 1,5-hexadiene, reaction (14), will be close to the high-pressure limit at 1160 K and 5 atm and  $k_{14} = 6 \times 10^{12} s^{-1}$  [52,53]. However, reaction (14) is in competition with addition reactions of H-atoms to give propene,  $k_{15} \sim 2 \times 10^{14} cm^3 mol^{-1} s^{-1}$  [54], and  $CH_3$  yielding 1-butene ( $1-C_4H_8$ )  $k_{16} \sim 1 \times 10^{13} cm^3 mol^{-1} s^{-1}$  [49,55]. No indication of 1,5-hexadiene ( $m/z$  82) was found in the experimental results, whereas 1-butene and propene were detected. In Figure 10, the 1-butene signal contains a small contribution from DI of 1-hexene at 10.70 eV (1.7% of  $m/z$  84 [27]). At 10.00 eV the DI of 1-hexene is only 0.12%.  $X_{eff}/time$  plots for 1-butene, 1,3-butadiene, propene and allene from 10.00 eV experiments are shown in Figure 12. The relative concentrations of the species in Figures 10 and 12 are similar, indicating the effect of DI at 10.70 eV was minimal. The  $X_{eff}$  of the allyl radical is also shown in Figure 12 and is similar to those of allene and 1,3-butadiene. At higher temperatures, the same trends in  $X_{eff}$  are observed except that 1-butene decomposes rapidly; see Figure S4. Simulation results from the MCHb and Fan models are shown in Figures 13 and 14. The MCHb model predicts that at 1160 K and 5 atm the  $X_{eff}$  of 1-butene and propene are roughly equal, with propene being formed slightly earlier than 1-butene. The mole fraction of 1,3-butadiene at 300  $\mu s$  is about a factor of two greater than that of allene but a factor of  $\sim 7$  lower than that of propene. The overall predictions of relative species concentrations are in good agreement with the experimental observations, Figures 10 and 12. On the other hand, the Fan model predicts ratios of  $X_{eff}$  as 1-butene/propene  $\sim 2$ , propene/1,3-butadiene  $\sim 3.5$  and 1,3-butadiene/allene  $\sim 3.5$ . At higher temperatures, similar differences exist between the results from both models. In the original works, the MCH [17] and Fan [11] models reproduced the experimental profiles for propene well. However, for 1-butene the Fan model reproduced the measurements well for the 0.04 bar experiments but overpredicted their 1 bar measurements by about a factor of 2. Conversely, the MCH model predicted Wang's 1-butene data well at 1 bar but underpredicted their measurements at 30 Torr by about a factor of 1.8.

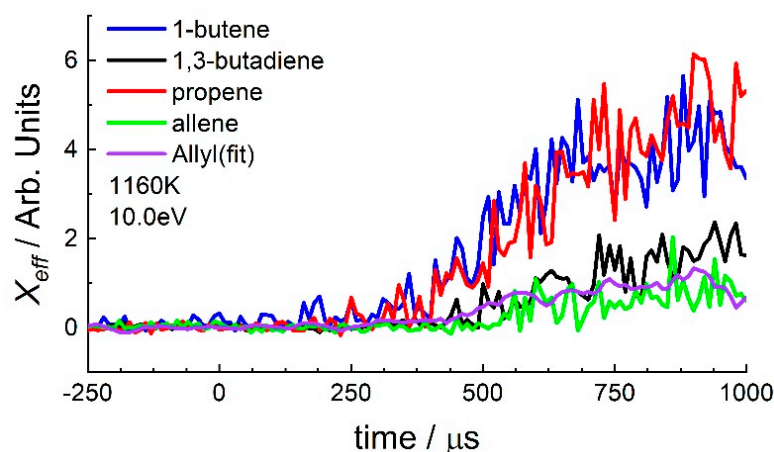


**Figure 12.** Effective concentration plots at 10.0 eV for several main products from the dissociation of 1-hexene; 1160 K and 4.4 bar.  $t = 0$  corresponds to formation of the reflected shock wave.

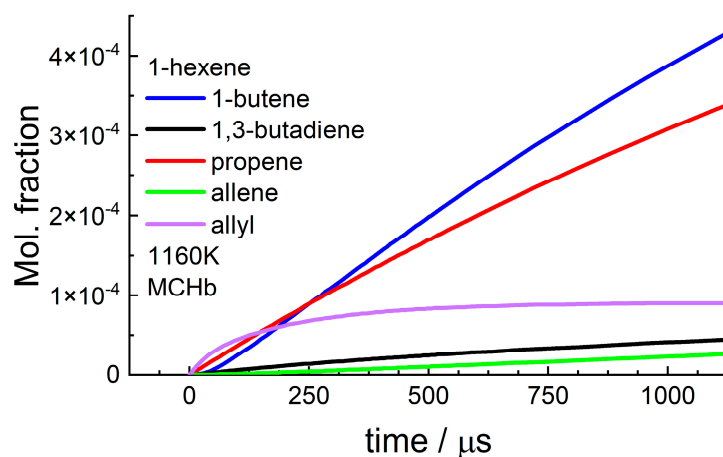


Figure 13. Simulation results for pyrolysis of 1-hexene with the MCHb model; 1160 K and 5 bar.

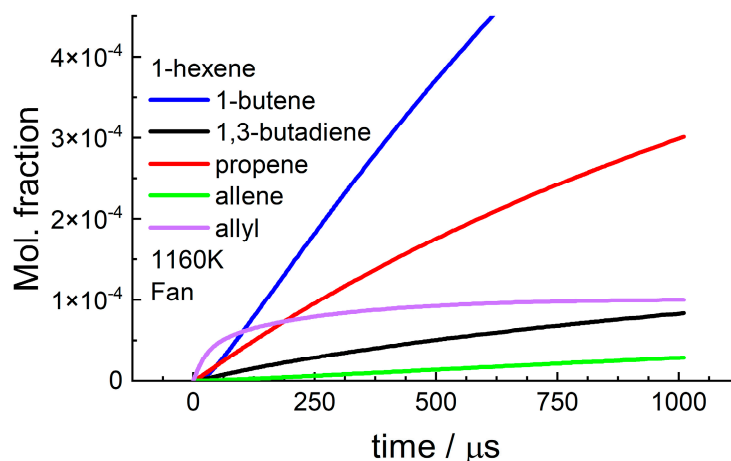


Figure 14. Simulation results for pyrolysis of 1-hexene with the Fan model; 1160 K and 5 bar.

While there are clear differences between the results of the two simulations, the agreement between the MCHb predictions and the experimental data may be fortuitous. The largest sources of uncertainty in the experimental  $X_{eff}$  are the photoionization cross-sections and assuming that  $M_d$ , the mass discrimination factor, is unity.  $M_d$  was discussed in [21] for the ANL-HRRST/TOF-MS, and for the small mass range in Figure 10,  $m/z$  40–56, this may result in an error of about 10–18% for  $m/z$  40 compared to  $m/z$  56 based on the  $M_d$  in [26,31]. For the molecular species in Figure 12, there are multiple measurements of the photoionization cross-sections. These were performed at different facilities by different groups. The various measurements for most species are in good agreement. However, for 1,3-butadiene a difference of a factor of two exists between the earlier measurement by Cool et al. [26] and the more recent one by Yang et al. [27]. Cool and Yang measured photoionization cross-sections for many molecules and, with the exception of 1,3-butadiene, good agreement was obtained between the datasets. The source of the difference in the 1,3-butadiene measurements is unknown [27] but the larger Yang et al. values, used here, are consistent with photoionization cross-sections for other  $C_4H_6$  molecules. The errors in  $X_{eff}$  for 1-butene, propene, 1,3-butadiene and allene due to uncertainties in cross-sections are estimated as 10–20% based on the source of a value. Thus, the uncertainties in  $X_{eff}$  for 1-butene and propene are not sufficient to account for the differences between the experimental results and Fan model simulations and support the agreement with the MCHb model.

Overall, there is good agreement between the MCHb model and the experiments. Conversely, the Fan model, which was specifically for 1-hexene, shows poor agreement.

Reaction flux diagrams from the MCHb model for 2% and 15% consumption of 1-hexene at 1160 K and 5 bar (Figures S8 and S9 of the supplementary material) show that 1-butene is formed from  $\text{CH}_3$  addition to allyl. In the MCHb model, propene is formed by four routes. The main path is the retroene dissociation of 1-hexene, reaction (6). Minor routes to propene include: H-atom addition to allyl, dissociation of *n*-propyl radicals and dissociation of radicals formed by abstraction of an H-atom from 1-hexene. In the Fan model, the retroene reaction is also mainly responsible for propene formation with a minor path from H-atom addition to the allyl radical being the only other contributor. Consequently, the differences in the predicted propene concentrations may largely be due to the different treatments of the *n*-propyl radical, discussed earlier, that effectively suppress reaction (12) in the Fan model. A simple test where the rate coefficient expressions in the Fan model for reactions (11) and (12) were replaced with those from the Wang model reduced the ratio of 1-butene/propene from a factor of 2 at 300  $\mu\text{s}$  to a factor of 1.4. Furthermore, in the MCHb model H-abstraction from 1-hexene appears to be more significant than in the Fan model and also contributes to the predicted propene concentration. Resolving the differences between the models with respect to the predictions of 1-butene and propene and the pressure dependency of the 1-butene formation will likely require detailed theoretical studies that are beyond the scope of this work.

#### 4.2. Cyclohexane

From prior studies, the initial dissociation of cyclohexane proceeds via reactions (1) and (2), yielding 1-hexene. Tsang identified 1-hexene as the major product [4] and Wang et al. [8] identified it in the photoionization spectrum for  $m/z$  84 where it was distinguishable from the isomer cyclohexane. In Figure 7, PIEs for  $m/z$  84 integrated over the first 100  $\mu\text{s}$  of reaction are shown from experiments at 1270 K and 1400 K. The IE of 1-hexene is 9.44 eV [32] and that of cyclohexane is 9.88 eV [32]. In Figure 7, there is no indication of an increase in signal in the region of 9.4 eV and at both temperatures the PIE spectra are essentially identical. Superficially, this might suggest that 1-hexene is not being formed in the ANL-HRRST. However, the current experiments were performed at nominal pressures of 9 bar whereas those of Wang et al. were at  $\sim 40$  mbar. At 1400 K and 8 bar  $k_3/k_1 = 45$  and  $k_3 = 4.9 \times 10^4 \text{ s}^{-1}$ . Whereas, at 1440 K and 40 mbar, Wang's conditions,  $k_3/k_1 = 7$  and  $k_3 = 1.7 \times 10^4 \text{ s}^{-1}$ . Thus, 1-hexene was probably not observed in the current work because it was consumed rapidly relative to the rate of formation.

Dissociation of 1-hexene produces H and  $\text{CH}_3$ . At 1400 K and 8 bar the mole fraction of  $\text{CH}_3$  is about 20 times greater than that of H. The rate coefficient for H attack on cyclohexane giving the cyclohexyl radical (reaction (7)) is  $> 2 \times 10^{13} \text{ cm}^3 \text{ mol}^{-1} \text{ s}^{-1}$ , whereas that for  $\text{CH}_3$  attack is  $9 \times 10^{10} \text{ cm}^3 \text{ mol}^{-1} \text{ s}^{-1}$ . Dissociation of cyclohexyl radicals and their products efficiently produces H-atoms, and the reactions of H-atoms will rapidly become more important than those of  $\text{CH}_3$  radicals.

In Figure 15, simulation results from the MCHb model for  $T = 1400 \text{ K}$  and 10 bar are shown for ethene, propene, allene + propyne ( $m/z$  40) and 1,3-butadiene. The corresponding experimental data are shown in Figure 4. At 300  $\mu\text{s}$  the concentrations of species relative to ethene, experimental with simulation in parentheses, are 1,3-butadiene 2 (2), propene 7 (8) and allene + propyne 7 (12). There is very good agreement between the simulations and experiments for the major species apart from allene + propyne. However,  $X_{\text{eff}}$  is dependent on  $\sigma_{x, \text{ev}}$  and the photoionization cross-section for propyne is approximately twice that for allene. The PIE curve for  $m/z$  40 is adequate for identifying the presence of allene and propyne but it is not sufficient for determining isomeric contributions to the  $X_{\text{eff}}$  curve. Consequently,  $\sigma_{x, \text{ev}}$  for allene was used to calculate  $X_{\text{eff}}$  and this is likely the source of the discrepancy between the model and experimental relative concentrations.

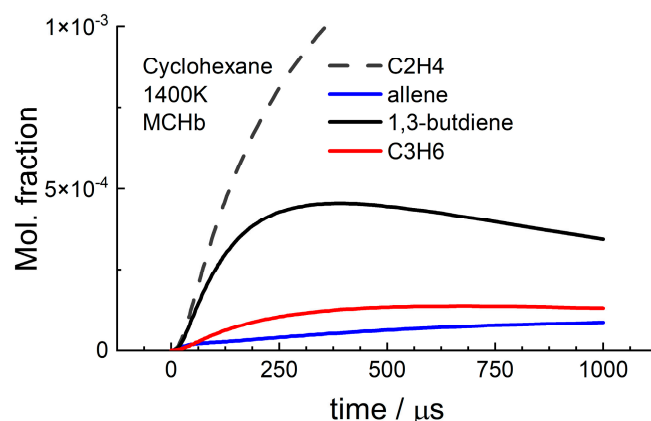


**Figure 15.** Simulation results with the MCH model for the pyrolysis of cyclohexane; 1400 K and 10 bar.

In addition to the dissociation paths for cyclohexyl discussed above, Tsang and Wang et al. have observed dehydrogenation products from sequential losses of H-atoms from cyclohexane. Gong et al. conducted a theoretical study of these processes [13] that are initiated by reaction (18) and cascade through reactions (19)–(22) resulting in benzene, which has been detected at long extents of reaction (Figures 2 and 3). Most of the species involved in this sequence have been identified in this work. In Figure 16, PIE spectra at 1400 K are shown for several species from  $m/z$  78–84 that are formed during the dehydrogenation of cyclohexane to benzene, reactions (18)–(21), including  $m/z$  82, 80 and 78 which correspond to cyclohexene ( $m/z$  82, IE 8.95 eV [32]), 1,3-cyclohexadiene ( $m/z$  80, IE 8.25 eV [33]) and benzene ( $m/z$  78, IE 9.24 eV [33]). It is possible that the  $m/z$  82 peak could be a combination of 1,3-cyclohexadiene and 1,4-cyclohexadiene. However, the IE of 1,4-cyclohexadiene is 8.82 eV [32] and there are no indications of a second species in the  $m/z$  82 PIE appearing around this energy.

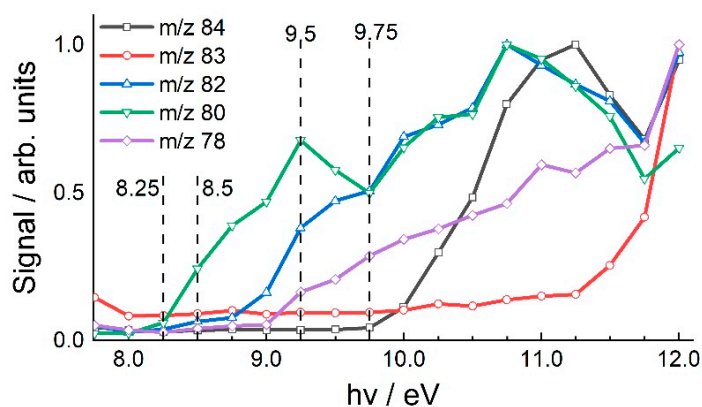
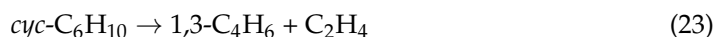
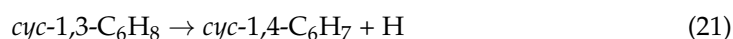


**Figure 16.** Photoionization spectra from dissociation of cyclohexane; 1400 K, 8 bar. The species are involved in the formation of benzene by dehydrogenation of cyclohexane.



In Figure 17, the signal/time profiles are shown for  $m/z$  83–78. The signals were not converted to  $X_{eff}$  due to a lack of a photoionization cross-section for the cyclohexyl radical. However, the figure shows cyclohexyl is formed early followed by cyclohexene, and then 1,3-cyclohexadiene and benzene appear nearly simultaneously.

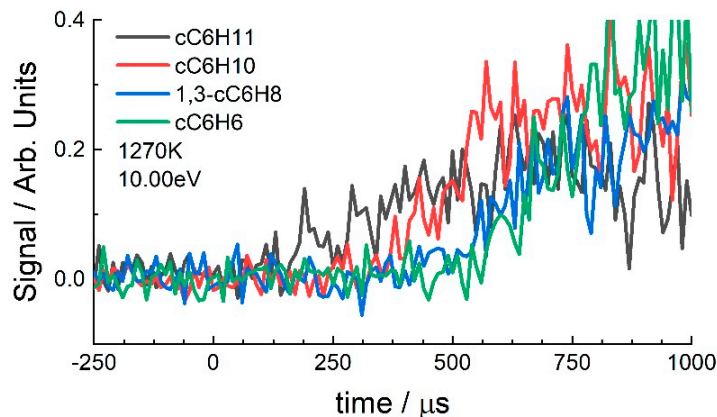


**Figure 17.** Species involved in the conversion of cyclohexane to benzene.  $T = 1270$  K,  $P = 7$  bar, no  $MgF_2$  filter.

## 5. Conclusions

The dissociation of cyclohexane and its initial decomposition product 1-hexene have been investigated at high temperatures and pressures. The data confirm the significant role of H-abstraction reactions in the pyrolysis of cyclohexane and the role of the cyclohexyl radical in the formation of benzene. A model for methylcyclohexane combustion from Wang et al. [17] was modified to update several sets of reactions and the revised model reproduced the relative concentrations of key stable species well. For 1-hexene a more recent model was available from Fan et al. [11] than that of Wang. However, while the modified Wang model satisfactorily reproduced the experimental 1-hexene results, the Fan model underpredicted the 1-butene:propene ratio. It is likely that the source of this disagreement is due to differences in the treatment of dissociation of the *n*-propyl radical and H abstraction from 1-hexene.

**Supplementary Materials:** The following supporting information can be downloaded at: <https://www.mdpi.com/article/10.3390/en16247929/s1>, Table S1: Photoionization cross-sections used in the analysis of mass spectra; Figure S1: Effective concentrations of propene from the pyrolysis of cyclohexane; Figure S2: Effective concentrations of allene + propyne from the pyrolysis of cyclohexane; Figure S3: Effective concentrations of ethene from the pyrolysis of cyclohexane; Figure S4: Main decomposition products from 1-hexene at 1360 K; Figure S5: Allyl radical concentration from the decomposition of 1-hexene at 1360 K; Figure S6: Fan model. Reaction flux diagram for 2% consumption of 1-hexene; 1160 K and 5 bar; Figure S7: Fan model. Reaction flux diagram for 15% consumption of 1-hexene; 1160 K and 5 bar; Figure S8: MCHb model. Reaction flux diagram for 2% consumption of 1-hexene; 1160 K and 5 bar; Figure S9: MCHb model. Reaction flux diagram for 15% consumption of 1-hexene; 1160 K and 5 bar; MCHb reaction mechanism.

**Author Contributions:** Conceptualization, R.S.T.; formal analysis, R.S.T., R.E.H. and C.B.; investigation, R.S.T. and C.B.; writing—original draft preparation, R.S.T. and C.B.; writing—review and editing, R.S.T., K.K. and C.B.; funding acquisition, R.S.T. and R.E.H. All authors have read and agreed to the published version of the manuscript.

**Funding:** This material is based on work supported by the U.S. Department of Energy, Office of Basic Energy Sciences, Division of Chemical Sciences, Geosciences, and Biosciences through the Argonne National Laboratory. Argonne is a U.S. Department of Energy laboratory managed by UChicago Argonne, LLC, under contract DE-AC0206CH11357. The ANL-HRRST experiments were conducted as part of the Argonne/Sandia Consortium on High Pressure Combustion Chemistry. This research used resources of the Advanced Light Source, which is a DOE Office of Science User Facility under

contract no. DE-AC02-05CH11231. The experiments were performed at beamline 9.0.2. REH was supported by the U.S. Department of Energy, Office of Science, Office of Workforce Development for Teachers and Scientists, Office of Science Graduate Student Research (SCGSR) program. The SCGSR program is administered by the Oak Ridge Institute for Science and Education for the DOE under contract number DE-SC0014664.

**Data Availability Statement:** Data are available from the corresponding author on request.

**Acknowledgments:** We are grateful to Franklin Goldsmith of Brown University for providing the pressure-dependent rate coefficients for reactions of C<sub>4</sub>H<sub>6</sub> isomers.

**Conflicts of Interest:** The authors declare no conflict of interest. The funders had no role in the design of the study; in the collection, analyses, or interpretation of data; in the writing of the manuscript; or in the decision to publish the results.

## References

1. Li, H.; Qiu, Y.; Wu, Z.; Wang, S.; Lu, X.; Huang, Z. Ignition delay of diisobutylene-containing multicomponent gasoline surrogates: Shock tube measurements and modeling study. *Fuel* **2019**, *235*, 1387–1399. [[CrossRef](#)]
2. Ren, S.; Kokjohn, S.L.; Wang, Z.; Liu, H.; Wang, B.; Wang, J. A multi-component wide distillation fuel (covering gasoline, jet fuel and diesel fuel) mechanism for combustion and PAH prediction. *Fuel* **2017**, *208*, 447–468. [[CrossRef](#)]
3. Pitz, W.J.; Mueller, C.J. Recent progress in the development of diesel surrogate fuels. *Prog. Energy Combust. Sci.* **2011**, *37*, 330–350. [[CrossRef](#)]
4. Tsang, W. Thermal Stability of Cyclohexane and 1-Hexene. *Int. J. Chem. Kinet.* **1978**, *10*, 1119–1138. [[CrossRef](#)]
5. Brown, T.C.; King, K.D.; Nguyen, T.T. Kinetics of primary processes in the pyrolysis of cyclopentanes and cyclohexanes. *J. Phys. Chem.* **1986**, *90*, 419–424. [[CrossRef](#)]
6. Kiefer, J.H.; Gupte, K.S.; Harding, L.B.; Klippenstein, S.J. Shock tube and theory investigation of cyclohexane and 1-hexene decomposition. *J. Phys. Chem. A* **2009**, *113*, 13570–13583. [[CrossRef](#)] [[PubMed](#)]
7. Peukert, S.; Naumann, C.; Braun-Unkhoff, M.; Riedel, U. The reaction of cyclohexane with H-atoms: A shock tube and modeling study. *Int. J. Chem. Kinet.* **2012**, *44*, 130–146. [[CrossRef](#)]
8. Wang, Z.; Cheng, Z.; Yuan, W.; Cai, J.; Zhang, L.; Zhang, F.; Qi, F.; Wang, J. An experimental and kinetic modeling study of cyclohexane pyrolysis at low pressure. *Combust. Flame* **2012**, *159*, 2243–2253. [[CrossRef](#)]
9. Khandavilli, M.V.; Djokic, M.; Vermeire, F.H.; Carstensen, H.-H.; Van Geem, K.M.; Marin, G.B. Experimental and Kinetic Modeling Study of Cyclohexane Pyrolysis. *Energy Fuels* **2018**, *32*, 7153–7168. [[CrossRef](#)]
10. Liszka, M.K.; Brezinsky, K. Variable high-pressure and concentration study of cyclohexane pyrolysis at high temperatures. *Int. J. Chem. Kinet.* **2019**, *51*, 49–73. [[CrossRef](#)]
11. Fan, X.; Wang, G.; Li, Y.; Wang, Z.; Yuan, W.; Zhao, L. Experimental and kinetic modeling study of 1-hexene combustion at various pressures. *Combust. Flame* **2016**, *173*, 151–160. [[CrossRef](#)]
12. Sirjean, B.; Glaude, P.A.; Ruiz-Lopez, M.F.; Fournet, R. Detailed Kinetic Study of the Ring Opening of Cycloalkanes by CBS-QB3 Calculations. *J. Phys. Chem. A* **2006**, *110*, 12693–12704. [[CrossRef](#)] [[PubMed](#)]
13. Gong, C.-M.; Li, Z.-R.; Li, X.-Y. Theoretical Kinetic Study of Thermal Decomposition of Cyclohexane. *Energy Fuels* **2012**, *26*, 2811–2820. [[CrossRef](#)]
14. Aribike, D.S.; Susu, A.A.; Ogunye, A.F. Mechanistic and mathematical modeling of the thermal decomposition of cyclohexane. *Thermochim. Acta* **1981**, *51*, 113–127. [[CrossRef](#)]
15. Zsély, I.G.G.; Varga, T.; Nagy, T.; Cserháti, M.; Turányi, T.; Peukert, S.; Braun-Unkhoff, M.; Naumann, C.; Riedel, U. Determination of rate parameters of cyclohexane and 1-hexene decomposition reactions. *Energy* **2012**, *43*, 85–93. [[CrossRef](#)]
16. Knepp, A.M.; Meloni, G.; Jusinski, L.E.; Taatjes, C.A.; Cavalotti, C.; Klippenstein, S.J. Theory, measurements, and modeling of OH and HO<sub>2</sub> formation in the reaction of cyclohexyl radicals with O<sub>2</sub>. *Phys. Chem. Chem. Phys.* **2007**, *9*, 4315–4331. [[CrossRef](#)]
17. Wang, Z.; Ye, L.; Yuan, W.; Zhang, L.; Wang, Y.; Cheng, Z.; Zhang, F.; Qi, F. Experimental and kinetic modeling study on methylcyclohexane pyrolysis and combustion. *Combust. Flame* **2014**, *161*, 84–100. [[CrossRef](#)]
18. Sikes, T.; Banyon, C.; Schwind, R.A.; Lynch, P.T.; Comandini, A.; Sivaramakrishnan, R.; Tranter, R.S. Initiation reactions in the high temperature decomposition of styrene. *Phys. Chem. Chem. Phys.* **2021**, *23*, 18432–18448. [[CrossRef](#)]
19. Tranter, R.S.; Lynch, P.T. A miniature high repetition rate shock tube. *Rev. Sci. Instrum.* **2013**, *84*, 094102. [[CrossRef](#)]
20. Lynch, P.T.; Troy, T.P.; Ahmed, M.; Tranter, R.S. Probing combustion chemistry in a miniature shock tube with synchrotron VUV photo ionization mass spectrometry. *Anal. Chem.* **2015**, *87*, 2345–2352. [[CrossRef](#)]
21. Randazzo, J.B.; Sivaramakrishnan, R.; Jasper, A.W.; Sikes, T.; Lynch, P.T.; Tranter, R.S. An experimental and theoretical study of the high temperature reactions of the four butyl radical isomers. *Phys. Chem. Chem. Phys.* **2020**, *22*, 18304–18319. [[CrossRef](#)] [[PubMed](#)]
22. Banyon, C.; Sikes, T.; Tranter, R.S. Reactions of propyl radicals: A shock tube–VUV photoionization mass spectrometry study. *Combust. Flame* **2021**, *224*, 14–23. [[CrossRef](#)]
23. Gaydon, A.G.; Hurler, I.R. *The Shock Tube in High-Temperature Chemical Physics*; Chapman and Hall: London, UK, 1963.

24. Anderson, J.D. *Modern Compressible Flow: With Historical Perspective*, 3rd ed.; McGraw-Hill Higher Education: Chicago, IL, USA, 2003.
25. Bandyopadhyay, B.; Kostko, O.; Fang, Y.; Ahmed, M. Probing Methanol Cluster Growth by Vacuum Ultraviolet Ionization. *J. Phys. Chem. A* **2015**, *119*, 4083–4092. [[CrossRef](#)] [[PubMed](#)]
26. Cool, T.A.; McIlroy, A.; Qi, F.; Westmoreland, P.R.; Poisson, L.; Peterka, D.S.; Ahmed, M. Photoionization mass spectrometer for studies of flame chemistry with a synchrotron light source. *Rev. Sci. Instrum.* **2005**, *76*, 094102. [[CrossRef](#)]
27. Yang, B.; Wang, J.; Cool, T.A.; Hansen, N.; Skeen, S.; Osborn, D.L. Absolute photoionization cross-sections of some combustion intermediates. *Int. J. Mass Spectrom.* **2012**, *309*, 118–128. [[CrossRef](#)]
28. Person, J.C.; Nicole, P.P. Isotope Effects in the Photoionization Yields and in the Absorption Cross Sections for Methanol, Ethanol, Methyl Bromide, and Ethyl Bromide. *J. Chem. Phys.* **2003**, *55*, 3390–3397. [[CrossRef](#)]
29. Robinson, J.C.; Sveum, N.E.; Neumark, D.M. Determination of absolute photoionization cross sections for isomers of C<sub>3</sub>H<sub>5</sub>: Allyl and 2-propenyl radicals. *Chem. Phys. Lett.* **2004**, *383*, 601–605. [[CrossRef](#)]
30. Holland, D.M.P.; Shaw, D.A. A study of the valence-shell photoabsorption, photodissociation and photoionisation cross-sections of allene. *Chem. Phys.* **1999**, *243*, 333–339. [[CrossRef](#)]
31. Zhou, Z.; Xie, M.; Wang, Z.; Qi, F. Determination of absolute photoionization cross-sections of aromatics and aromatic derivatives. *Rapid Commun. Mass Spectrom.* **2009**, *23*, 3994–4002. [[CrossRef](#)]
32. Lias, S.G.; Bartmess, J.E.; Liebman, J.F.; Holmes, J.L.; Levin, R.D.; Mallard, W.G. Ion Energetics Data. In *NIST Chemistry WebBook, NIST Standard Reference Database Number 69*; Linstrom, J., Mallard, W.G., Eds.; National Institute of Standards and Technology: Gaithersburg, MD, USA, 2023. [[CrossRef](#)]
33. Demeo, D.A.; El-Sayed, M.A. Ionization Potential and Structure of Olefins. *J. Chem. Phys.* **2003**, *52*, 2622–2629. [[CrossRef](#)]
34. Li, Y. Available online: <http://flame.nslr.ustc.edu.cn/database/data.php?wid=346> (accessed on 1 June 2023).
35. Wang, J.; Yang, B.; Cool, T.A.; Hansen, N.; Kasper, T. Near-threshold absolute photoionization cross-sections of some reaction intermediates in combustion. *Int. J. Mass Spectrom.* **2008**, *269*, 210–220. [[CrossRef](#)]
36. Cool, T.A.; Nakajima, K.; Mostefaoui, T.A.; Qi, F.; McIlroy, A.; Westmoreland, P.R.; Law, M.E.; Poisson, L.; Peterka, D.S.; Ahmed, M. Selective detection of isomers with photoionization mass spectrometry for studies of hydrocarbon flame chemistry. *J. Chem. Phys.* **2003**, *119*, 8356–8365. [[CrossRef](#)]
37. Schoen, R.I. Absorption, Ionization, and Ion-Fragmentation Cross Sections of Hydrocarbon Vapors under Vacuum-Ultraviolet Radiation. *J. Chem. Phys.* **1968**, *37*, 2032–2041. [[CrossRef](#)]
38. Holland, D.M.P.; Shaw, D.A.; Hayes, M.A.; Shpinkova, L.G.; Rennie, E.E.; Karlsson, L.; Baltzer, P.; Wannberg, B. A photoabsorption, photodissociation and photoelectron spectroscopy study of C<sub>2</sub>H<sub>4</sub> and C<sub>2</sub>D<sub>4</sub>. *Chem. Phys.* **1997**, *219*, 91–116. [[CrossRef](#)]
39. Dalmiya, A.; Mehta, J.M.; Tranter, R.S.; Lynch, P.T. High pressure, high flow rate batch mixing apparatus for high throughput experiments. *Rev. Sci. Instrum.* **2021**, *92*, 114104. [[CrossRef](#)] [[PubMed](#)]
40. Sikes, T.; Tranter, R.S. Frhodo: A program for simulating chemical kinetic measurements and optimizing kinetic mechanisms. *Combust. Flame* **2022**, *257*, 112509. [[CrossRef](#)]
41. Wang, Q.-D. Theoretical studies of unimolecular thermal decomposition reactions of n-hexane and n-hexene isomers. *Comput. Theor. Chem.* **2017**, *1115*, 45–55. [[CrossRef](#)]
42. Lockhart, J.P.A.; Goldsmith, C.F.; Randazzo, J.B.; Ruscic, B.; Tranter, R.S. An Experimental and Theoretical Study of the Thermal Decomposition of C<sub>4</sub>H<sub>6</sub> Isomers. *J. Phys. Chem. A* **2017**, *121*, 3827–3850. [[CrossRef](#)]
43. Miller, J.A.; Klippenstein, S.J. Dissociation of propyl radicals and other reactions on a C<sub>3</sub>H<sub>7</sub> potential. *J. Phys. Chem. A* **2013**, *117*, 2718–2727. [[CrossRef](#)]
44. Goodwin, D.G.; Speth, R.L.; Moffat, H.K.; Weber, B.W. Cantera: An Object-Oriented Software Toolkit for Chemical Kinetics, Thermodynamics, and Transport Processes, Version 2.6.0. 2022. Available online: <https://zenodo.org/records/6387882> (accessed on 1 June 2023).
45. PyDot. Available online: <https://pypi.org/project/pydot/> (accessed on 1 June 2023).
46. GraphViz. Available online: <https://www.graphviz.org/> (accessed on 1 June 2023).
47. Kiefer, J.H.; Mudipalli, P.S.; Sidhu, S.S.; Kern, R.D.; Jursic, B.S.; Xie, K.; Chen, H. Unimolecular Dissociation in Allene and Propyne: The Effect of Isomerization on the Low-Pressure Rate. *J. Phys. Chem. A* **1997**, *101*, 4057–4071. [[CrossRef](#)]
48. Houle, F.A.; Beauchamp, J.L. Detection and investigation of allyl and benzyl radicals by photoelectron spectroscopy. *J. Am. Chem. Soc.* **1978**, *100*, 3290–3294. [[CrossRef](#)]
49. Tsang, W. Chemical kinetic database for combustion chemistry part V. Propene. *J. Phys. Chem. Ref. Data* **1991**, *20*, 222–274. [[CrossRef](#)]
50. Hansen, N.; Merchant, S.S.; Harper, M.R.; Green, W.H. The predictive capability of an automatically generated combustion chemistry mechanism: Chemical structures of premixed iso-butanol flames. *Combust. Flame* **2013**, *160*, 2343–2351. [[CrossRef](#)]
51. Fernandes, R.X.; Gird, B.R.; Hippler, H.; Kachiani, C.; Striebel, F. Shock wave study on the thermal unimolecular decomposition of allyl radicals. *J. Phys. Chem. A* **2005**, *109*, 1063–1070. [[CrossRef](#)]
52. Lynch, P.T.; Annesley, C.J.; Aul, C.J.; Yang, X.; Tranter, R.S. Recombination of allyl radicals in the high temperature fall-off regime. *J. Phys. Chem. A* **2013**, *117*, 4750–4761. [[CrossRef](#)] [[PubMed](#)]
53. Georgievskii, Y.; Miller, J.A.; Klippenstein, S.J. Association rate constants for reactions between resonance-stabilized radicals: C<sub>3</sub>H<sub>3</sub> + C<sub>3</sub>H<sub>3</sub>, C<sub>3</sub>H<sub>3</sub> + C<sub>3</sub>H<sub>5</sub>, and C<sub>3</sub>H<sub>5</sub> + C<sub>3</sub>H<sub>5</sub>. *Phys. Chem. Chem. Phys.* **2007**, *9*, 4259. [[CrossRef](#)]

54. Harding, L.B.; Klippenstein, S.J.; Georgievskii, Y. On the combination reactions of hydrogen atoms with resonance-stabilized hydrocarbon radicals. *J. Phys. Chem. A* **2007**, *111*, 3789–3801. [[CrossRef](#)]
55. Knyazev, V.D.; Slagle, I.R. Kinetics of the Reactions of Allyl and Propargyl Radicals with CH<sub>3</sub>. *J. Phys. Chem. A* **2001**, *105*, 3196–3204. [[CrossRef](#)]

**Disclaimer/Publisher's Note:** The statements, opinions and data contained in all publications are solely those of the individual author(s) and contributor(s) and not of MDPI and/or the editor(s). MDPI and/or the editor(s) disclaim responsibility for any injury to people or property resulting from any ideas, methods, instructions or products referred to in the content.